Nanoscale

Accepted Manuscript

This article can be cited before page numbers have been issued, to do this please use: Y. Huang, K. Xu, Z. Wang, T. A. Shifa, Q. Wang, F. Wang, C. Jiang and J. He, *Nanoscale*, 2015, DOI: 10.1039/C5NR05989E.

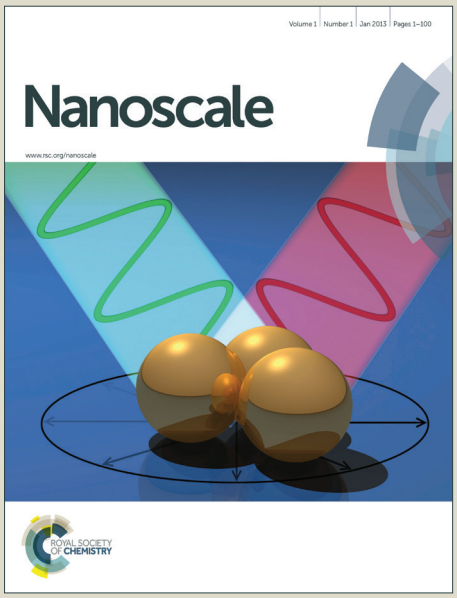

This is an *Accepted Manuscript*, which has been through the Royal Society of Chemistry peer review process and has been accepted for publication.

Accepted Manuscripts are published online shortly after acceptance, before technical editing, formatting and proof reading. Using this free service, authors can make their results available to the community, in citable form, before we publish the edited article. We will replace this *Accepted Manuscript* with the edited and formatted *Advance Article* as soon as it is available.

You can find more information about *Accepted Manuscripts* in the Information for Authors.

Please note that technical editing may introduce minor changes to the text and/or graphics, which may alter content. The journal's standard Terms & Conditions and the Ethical guidelines still apply. In no event shall the Royal Society of Chemistry be held responsible for any errors or omissions in this *Accepted Manuscript* or any consequences arising from the use of any information it contains.

ROYAL SOCIETY OF CHEMISTRY

www.rsc.org/nanoscale

View Article Online
DOI: 10.1039/C5NR05989E

Nanoscale

ARTICLE

Designing Shape Evolution of $SnSe_2$ Nanosheets and their Optoelectronic Property

Received 00th January 20xx,
Accepted 00th January 20xx

DOI: 10.1039/x0xx00000x

www.rsc.org/

Yun Huang, Kai Xu, Zhenxing Wang, Tofik Ahmed Shifa, Qisheng Wang, Feng Wang, Chao Jiang and Jun He*

Layered chalcogenide materials (LCMs) are emerging materials in recent years for their great potential in application of electronics and optoelectronics. As a member of LCMs, $SnSe_2$, an n-type semiconductor with a band gap ~1.0 eV，is of great value to explore. In this paper, we develop a facile CVD method, for the first time, to synthesize diverse shaped $SnSe_2$ and square SnSe nanosheets (NSs) on SiO_2/Si substrates. To the best of our knowledge, the thickness of as-grown $SnSe_2$ is among the thinnest ones synthesized by CVD methods on various substrates. What's more, photodetectors are fabricated to investigate the optoelectronic properties of $SnSe_2$. The on/off ratio as photo switches reaches 100 under illumination of 800 nm laser. This work will pave a new pathway to synthesize LCMs nanostructures, shed light on the shape evolution during growth process and expand the candidates for high performance optoelectronic devices.

Introduction

As complements to graphene, two-dimensional (2D) LCMs, especially MX_2 (M=Mo, W, Sn, Ti, Zr, Hf, Nb, Ta, and X = S, Se), have drawn tremendous attention in recent years. Compared to graphene, these MX_2 materials own band gaps in the range of 1-2 eV, which are suitable for digital electronic applications.[1-3] Besides, the weak van der Waals interaction between adjacent layers renders monolayer or few multilayer LCMs available. Based on these features, plenty of gorgeous progresses have been achieved for synthesis and applications of LCMs. For instance, monolayer MoS_2 have been realized by mechanical exfoliation[4]. Chemical vapor deposition (CVD) method could synthesize monolayer MoS_2 with wafer scale.[5] The measured carrier mobility of MoS_2 in extremely low temperature can be as high as 34,000 $cm^2V^{-1}s^{-1}$.[6] Atomic p-n diodes at the ultimate thickness limit were successfully realized on monolayer WSe_2.[7] Meanwhile, other members of LCMs, such as SnS_2, exhibits superior properties as ultrafast phototransistors with response time as short as 5 μs.[8] The responsivity of phototransistors based on GaTe could be as high as 800 A/W.[9] High performance field effect transistors based on WSe_2 and $MoTe_2$ could go through a transfer from hole conduction to electron conduction by gate voltage regulation.[10, 11] During the deep excavation of LCMs, fancy devices with high performances emerge, which significantly put forward the innovation and development of semiconductor industry.

As an emerging member of LCMs, $SnSe_2$ is of great value to explore. It is an n-type semiconductor with a band gap ~1.0 eV, which normally crystallizes in a hexagonal structure with two layers of Se atoms sandwiching a Sn layer.[12] So far, $SnSe_2$ nanostructures have been exploited in applications of phase change memory,[13] lithium ion batteries,[14] high drive current FET[12, 15] and so on. Thin films of $SnSe_2$ could be obtained by mechanical exfoliation from bulk or solvothermal approach.[12, 15-18] But these methods fail to synthesize $SnSe_2$ NSs with large scale and high crystalline quality. In contrast, CVD is universally acknowledged as an effective approach to complement both. To the best of our knowledge, owing to the relatively thick thickness, the $SnSe_2$ synthesized by CVD method reported do not exhibit their superiorities as layer materials to fabricate electrical or optoelectronic devices. [19, 20] Ultrathin $SnSe_2$ NSs synthesized by CVD with thickness lower than 10 nm and their potential application as photodetector have not been reported yet.

Herein we present a recipe to successfully synthesize $SnSe_2$ NSs on SiO_2/Si substrates. Scanning electron microscope (SEM), Raman spectroscopy, electron energy dispersive X-ray spectroscopy (EDX) and transmission electron microscope (TEM) were employed to characterize the composition and crystal structures of the NSs. The thickness of as-grown $SnSe_2$ NSs, which is measured with an atomic force microscope (AFM), could be lower than 10 nm with the lateral size ~ 5 μm. In particular, the products could evolve from square SnSe NSs to varied shapes of $SnSe_2$, successively shaping as hexagon, truncated triangles and triangle along the decreasing direction of temperature gradient. Unlike $SnSe_2$, layered SnSe has an

CAS Key Laboratory of Nanosystem and Hierarchical Fabrication, National Center for Nanoscience and Technology, 100190, Beijing, P. R. China.
E-mail: hej@nanoctr.cn
Electronic Supplementary Information (ESI) available: more information about XRD and AFM data. See DOI: 10.1039/x0xx00000x

View Article Online
DOI: 10.1039/C5NR05989E

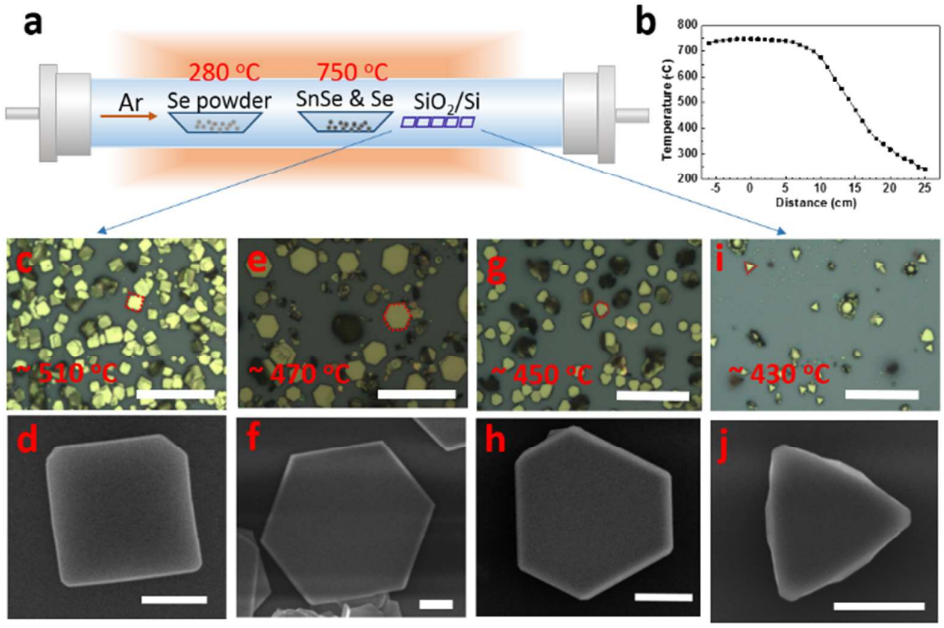

Fig. 1 The experimental setting and various NSs grown on SiO_2/Si substrates. (a) The schematic of the experimental setups. (b) The temperature gradient in the furnace. The middle of the second heating zone is defined as the origin. (c, e, g and i) The OM images of as-grown NSs. Scale bar: 30 µm. (d, f, h and i) The corresponding SEM images of NSs. Scale bar: c, 0.5 µm; e, g and i, 2 µm.

orthorhombic crystal structure.[21] Grown models are developed to figure out the mechanism of NSs evolution. We also fabricate photodectors based on as-grown $SnSe_2$ NSs and study their optoelectronic properties. Under illumination of 800 nm laser, the on/off ratio of photo switch could be ~100. Our study may provide a method to synthesize LCMs with designed shape and broaden the candidates for high performance photodetectors.

Results and discussion

The experimental setup and morphology of as grown nanostructures are depicted in Fig. 1. In contrast to the previous work,[20] cleaned SiO_2/Si substrates were placed downstream from the second heating zone ~14 -18cm. Fig. 1b shows the temperature gradient of the furnace. As the temperature of substrates declines, the shape of the deposited NSs resembles square, hexagonal, truncated triangular and triangular in sequence, which are displayed in Fig. 1c-j. Along the flow direction, we first observed square NSs on substrates at ~ 510 °C. The NSs' size could augment as the dosage of SnSe powder increases. Furthermore, by adjusting the temperature and precursor dose for experimental settings, the dominating shape of NSs can be controlled. For example, hexagonal or half-hexagonal $SnSe_2$ NSs would be the majority when use the mixed powder as the precursor only. The reason for this trend will be discussed later.

To confirm the crystallinity and composition of NSs imaged by OM and SEM in Fig. 1, further characterization was made by Raman spectroscopy and EDX. Accordingly, Fig. 2a and 2b show the Raman and EDX spectrums corresponding to the square NSs. As illustrated in Fig. 2a, the three intense Raman peaks at 110.3 cm^{-1} (B_{3g}), 131.9 cm^{-1} (A_g), and 149.8 cm^{-1} (A_g), can be attributed to the characteristics features of SnSe.[21-23] Moreover, the high crystallinity of SnSe NSs is apparent from the uniform color contrast and high intensity of the Raman mapping (B_{3g} phonon mode) in inset of Fig. 2a. We further demonstrate the Sn: Se atomic ratio of the NSs close to 1:1 by EDX, which are illustrated in Fig. 2b. The hexagonal, truncated triangular and triangular NSs are characterized in similar ways. Fig.s 2c, e and g respectively exhibit their Raman spectra. The intense peaks at ~118.5 cm^{-1} and ~185.2 cm^{-1} correspond to A_{g1} and E_g mode of $SnSe_2$.[17] The Raman mappings of A_{g1} mode in the insets are in homogeneous intensity, revealing the good crystalline quality of the NSs. As it is evident from their respective EDX, the atomic ratios close to 1:2 agree with their expected stoichiometric composition. Based on the above critical observations, we believe that we successfully synthesized square SnSe and various shaped $SnSe_2$ NSs on SiO_2/Si substrates.

Transmission electron microscope (TEM) and atomic force microscope (AFM) are used to further evaluate the crystal structure and thickness of NSs we synthesized. Fig. 3a presents a TEM image of SnSe dispersed onto a holey carbon film. The regular diffraction fringes (HRTEM) and corresponding selected electron diffraction pattern (SAED) shown in Fig. 3b and c, indicating the single crystal nature and high crystallinity of as grown SnSe NSs. The lattice spacing ~ 4.25 Å and corresponding orthogonally symmetric SAED pattern are in great agreement with the orthorhombic crystal structure of SnSe NS. Fig. 3e and i manifest TEM images of a hexagonal and

View Article Online
DOI: 10.1039/C5NR05989E

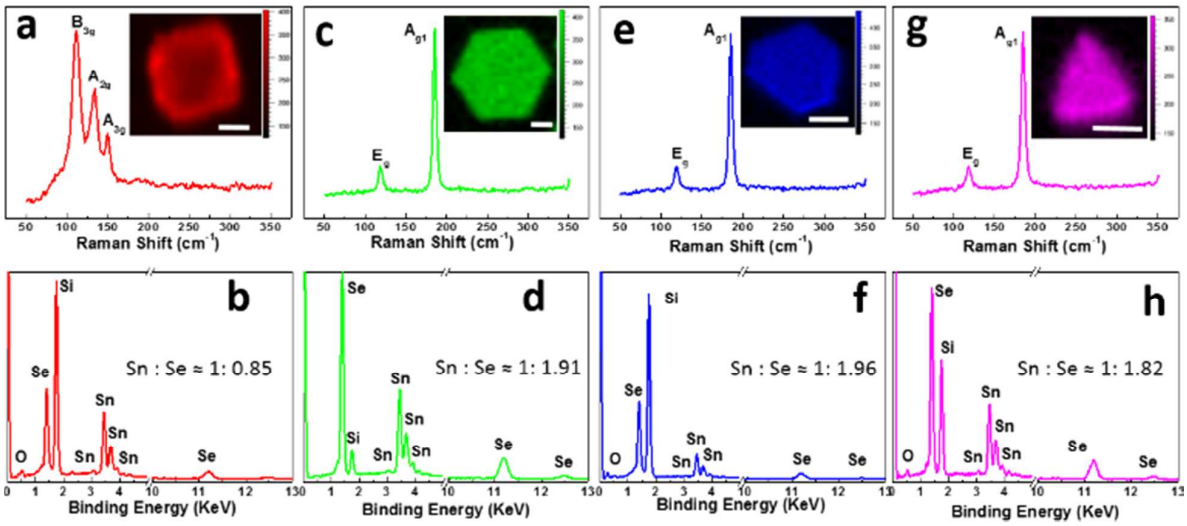

Fig. 2 Raman and EDX spectrums of various shaped NSs. (a, c, e and g) The Raman spectrum with an excitation laser of 532 nm of square, hexagonal, truncated triangular and triangular NSs. Inset: the corresponding image of Raman mapping of the most intensive Raman peak. Scale bar: 2 μm. (b, d, f and h) the corresponding EDX spectrums of as-grown NSs.

a half-hexagonal $SnSe_2$ NS. The corresponding HRTEM and SAED are depicted in Fig. 3f, g, j, and k, with the lattice spacing of 3.29 Å and 3.31 Å indexed to (100) plane, and the zone axis of hexagonally symmetric SAED spots assigned to [001] direction. These results demonstrate the synthesized $SnSe_2$ NSs are single crystalline with high crystal quality. The AFM image displayed in Fig. 3d, h and l demonstrate that the thickness of as grown smooth NSs is ~ 153.3 nm, 73.8 nm and 9.4 nm. The thin $SnSe_2$ NSs are mainly found at the downstream locations of the substrates, where nucleate sites are fewer than the edge of upstream.[24] More AFM data of the thin NSs are shown in Fig. S1. The X-Ray Diffraction (XRD) results of as-grown NSs are depicted in Fig. S2. To the best of our knowledge, this is the first report to come up with ultrathin $SnSe_2$ NSs with thickness bellow 10 nm. Our CVD approach, therefore, resulted in the thinnest ever reported $SnSe_2$ NSs endowing immense application in electronic and optoelectronic devices.

Generally, only one kind of material other than multiple ones would be obtained under a certain growth condition. However, during our experimental process, materials with two kinds of component in various shapes are synthesized. It is of great value to understand the growth mechanism during this process, which may help us controllably synthesize LCMs in the future. As shown in Fig. 4a, the growth process may experience three steps: (1) the sublimation of source materials at proper temperature and their carriage by carrier gas, (2) adsorption and desorption of source materials atoms onto substrates, (3) nucleation and reaction of adsorbed atoms on substrates. It is easy to understand that the deposition rate differs between different atoms. On substrates of higher temperatures, more active atoms would quickly desorb into the carrier gas. Accordingly, the ratio of deposited atoms would vary as the temperature of substrates changes. According to the results of our experiment, on substrates of higher temperature, adsorbed selenium atoms incline to quickly desorb into the carrier gas, thus SnSe nucleates and grows into square NS under proper gas flow and pressure. When the temperature of substrates decreases, the amount of desorbed selenium atoms declines and there are enough adsorbed ones to react with Sn. As a result, $SnSe_2$ NSs are synthesized. This trend is in agreement with a former report, in which SnSe would be deposited by selenization Sn film from 530 °C to 570 °C, while $SnSe_2$ would be deposited from 430 °C to 470 °C.[25]

The phenomenon of shape evolution may also confirm this trend. It has been established that the most commonly and energetically favored edge structures of MoS_2 are Mo zigzag (Mo-zz) terminations and S zigzag (S-zz) terminations,[26, 27] which alternatively constructs the six edges of a hexagonal shaped MoS_2 NS. Since $SnSe_2$ own the same hexagonal crystal structure with MoS_2, in which Sn (Se) atoms replace the position of Mo (S) atoms, it should follow a similar principle. For Sn-zz terminations, each Sn atom has two dangling bonds, while for Se-zz terminations, the dangling bonds become one. This difference may result in the distinct chemical activity of those terminations, which may further lead to their diverse growth rates. In consequence, the shape of crystals evolves, as shown in Fig. 4b.

During the growth process of our experiment, the concentration of Se atoms deposited on the substrates plays a significant role in the shape evolution. As the temperature of substrates decreases, more and more Se atoms deposited. At surface of substrates where Se atoms are sufficient, the Sn-zz terminations become more active to meet and bond with Se atoms around, thus grow faster than Se-zz terminations. In consequence, the Sn-zz terminations become shorter and shorter (shaping like truncated triangles) and eventually

View Article Online
DOI: 10.1039/C5NR05989E

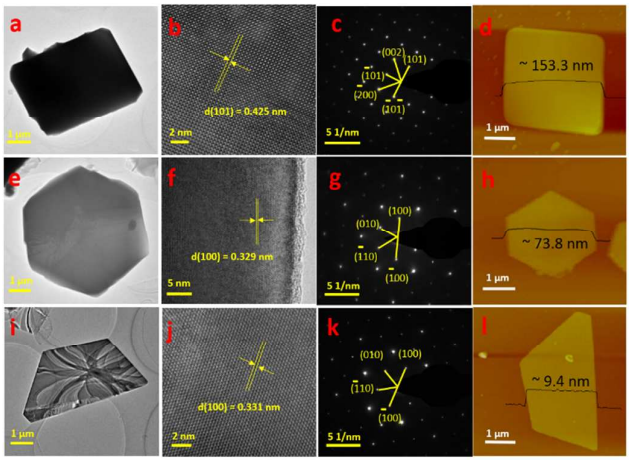

Fig. 3 The TEM and AFM images of NSs synthesized. The low magnification bright field TEM (a, e and i), HRTEM (b, f and j), corresponding SEAD patterns (c, g and k) and AFM (d, h and l) images of a square SnSe NS, a hexagonal $SnSe_2$ NS and a half-hexagonal $SnSe_2$ NS dispersed onto holey carbon films.

disappear (shaping like triangles) as the temperature of substrates decrease. The effect of precursor amounts on the shape evolution attest the assumption, too. The reduction of Se powder (Se precursor) and SnSe powder (Sn precursor) leads to the formation of hexagonal and triangular shapes respectively. This phenomenon is also observed for other LCMs, such as MoS_2,[28, 29] which further corroborates our assumption. Moreover, the pressure during the gas flow also plays significant role in affecting the shape of $SnSe_2$ NSs. The regular NSs is achieved only under pressure 220~230 Pa in our experimental settings. Otherwise, the products tend to form into amorphous SnSe and $SnSe_2$ domains.

We further explore the optoelectronic properties of $SnSe_2$ NSs. A photo detector device based on as-grown $SnSe_2$ NSs is fabricated through a standard EBL process, following by thermal deposition of Cr/Au (5 nm/80 nm) as electrodes. Fig. 5a displays an AFM image of the detector with a $SnSe_2$ NS ~21.1 nm. To examine the performance of the device, we put it under illumination of 800 nm laser and measure its optoelectronic properties at 140 K to diminish the effect of laser heating. As depicted in Fig. 5b, the detector exhibits a monotonically increasing photocurrent as the incident power of illumination increases from 0.227 W/mm^2 to 4.380 W/mm^2. We also calculate the responsivity (R_λ) and photogain (G) from following equations:[9, 30]

$$R_\lambda = I_{ph}/PS,$$
$$\mathrm{G} = I_{ph}h\nu/qPS$$

where I_{ph} is the photocurrent, h is the Planck constant, ν and P is the incident light frequency and power respectively, and S is the effective illuminated area. Fig. 5c shows the relationship between them and the incident beam power. Accordingly, the R_λ can reach ~1900 mA/W and the on/off ratio of this device as photos witches could be 100. To evaluate the performance of our fabricated $SnSe_2$ photodetectors, we list the figure-of-merit of some devices based on other 2D materials, as shown in Table 1.[31-36] The measured responsivity of $SnSe_2$ photodetector is acceptable among 2D materials, and the on/off ratio of photo switch is among the largest ones in the table, indicating the potential of $SnSe_2$ NSs as high performance photo switches.

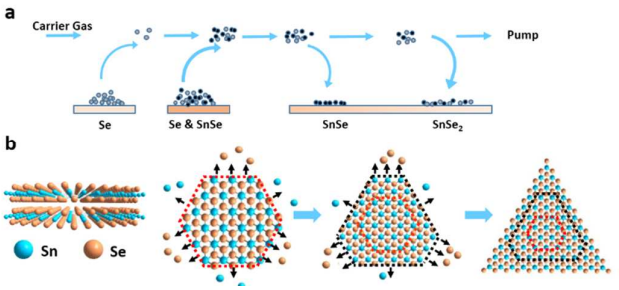

Fig. 4 The schematic of the growth mechanism. (a) A schematic illustrates the major three steps during the vapor deposition process. (b) A simple model to expound the shape evolution.

Conclusions

In conclusion, we develop a one-step method to synthesize SnSe and $SnSe_2$ NSs on SiO_2/Si substrates. Along the decreasing direction of temperature gradient, the shape of as-grown NSs changes from square SnSe, hexagonal and truncated triangular $SnSe_2$ to triangular $SnSe_2$ by controlling the amount of source materials and the pressure during the growth process. Models are proposed to explain the shape evolution under our experimental setups. Photodetectors based on as-grown $SnSe_2$ NSs exhibit a high photo switch on/off ratio ~100 under illumination of 800 nm laser. Our work will open up a new way in the synthesis of LCMs and broaden the building blocks for high performance optoelectronic devices.

Experimental

Synthesis of SnSe and $SnSe_2$ NSs on SiO_2/Si substrates. A horizontal vacuum tube furnace with two heating zones is used for the synthesis process. The quartz tube is in diameter of 2 in. and length of 40 in. Se powder (99.999%, Alfa Aesar) and SnSe powder grinded from bulk (99.999%, Alfa Aesar) served as the precursors. Prior to the growth, 300 nm SiO_2/Si substrates (~1×1 cm^2) were cleaned by a piranha solution at 120 °C for 2 h followed by rinsing in deionized water and drying in fluid nitrogen. As shown in Fig. 1a, during a typical growth process, 0.1 g Se powder were placed in a quartz boat in the middle of the first heating zone. 0.01 g SnSe powder mixed with 0.3 g Se powder were placed in another quartz boat in the middle of the second heating zone. The cleaned SiO_2/Si substrates were placed downstream from the second heating zone ~14 -18cm. After flushing with Ar gas three times and pumping to a vacuum lower than 1 Pa, the gas flow of Ar was controlled at 50 sccm. Then, the Se powder were heated up to 250 °C in 10 minutes to provide an atmosphere of selenide before the mixed powder were heated up to 750 °C

View Article Online
DOI: 10.1039/C5NR05989E
Nanoscale ARTICLE

Table 1. Comparison of Figures-of-Merit for Photodetecotrs Based on 2D Materials

Material	Measurement conditions	Responsivity (mA/W)	On/off ratio	reference
>1L $SnSe_2$	V_{ds} = 1 V, V_g = 0 V, P = 3.44 W, λ = 800 nm	1.9×10^3	100	This work
>1L b-P	V_{ds} = 0.2 V, V_g = 0 V, P = 10 nW, λ = 640 nm	4.8	< 10	31
>1L MoS_2	V_{ds} = 1 V, V_g = -2 V, P = 50 mW/cm^2, λ = 633 nm	110	~ 100	32
1L $MoSe_2$	V_{ds} = 10 V, V_g = 0 V, P = 100 mW/cm^2, λ = 532 nm	13	~ 10	33
1L MoS_2	V_{ds} = 1 V, V_g = 41 V, P = 0.13 mW/cm^2, λ =532 nm	2.2×10^6	--	34
1L WS_2	V_{ds} = 30 V, V_g = 0 V, P = 0.05 mW/cm^2, λ = 633 nm	1.3×10^4	~ 30	35
>1L ReS_2	V_{ds} = 0.05 V, V_g = -10 V, P = 25 nW, λ = 633 nm	1.6×10^4	2.8	36

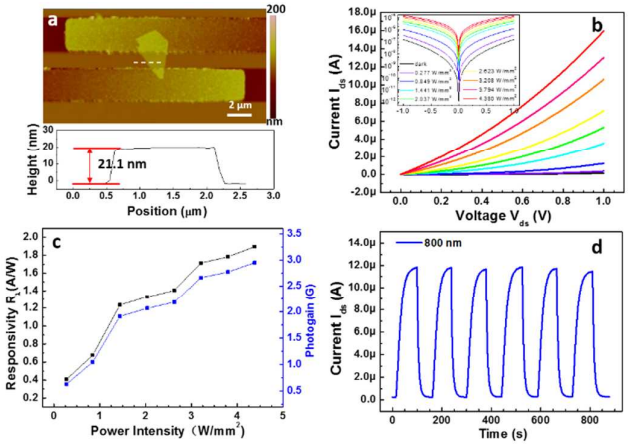

Fig. 5 Characteristics of a photodetector based on as-grown $SnSe_2$ NSs and its property under illumination of 800 nm laser at 140K. (a) The AFM image along with cross section height profiles of the $SnSe_2$ NS as a photodetector. (b) Transfer curves at different incident power illuminations in linear coordinates. Inset: The responding curves in logarithmic coordinates. (c) The relationship of calculated responsivity and photogain with the power intensity. (d) Time response of the device under illumination as a photoswitch.

in 15 minutes. The growth process was sustained for 30minutes. After that, the furnace was naturally cooled to room temperature. Square SnSe and varied shapes of $SnSe_2$ NSs were deposited on SiO_2/Si in different location.

Characterizations for SnSe and $SnSe_2$ NSs. The morphology of SnSe and $SnSe_2$ NSs were characterized an SEM (FESEM, Hitach S-4800) and an AFM (Veeco Multimode). Raman spectroscopy (Renishaw InVia, 532 nm excitation laser) and EDX attached to the SEM were used to further characterize the composition of experimental products. The crystal structure information were obtained by a TEM (Tecnai F20).

Device fabrication and electrical measurement. The as-grown thin $SnSe_2$ NSs were transferred onto heavily p-doped 300 nm SiO_2/Si substrates. A standard e-beam lithography (EBL) process was used to define the electrical metal electrodes.

After that, Cr/Au (5 nm/ 80 nm) metal electrodes were deposited by thermal evaporation. A probe station (Lakeshore, TTP4), a semiconductor characterization system (Keithley 4200) and an 800 nm laser were utilized for optoelectronic measurements.

Acknowledgements

This work at National Center for Nanoscience and Technology was supported by 973 Program of the Ministry of Science and Technology of China (No. 2012CB934103), the 100-Talents Program of the Chinese Academy of Sciences (No. Y1172911ZX), the National Natural Science Foundation of China (Nos. 21373065 and 61474033) and Beijing Natural Science Foundation (No. 2144059).

Notes and references

1. S. Z. Butler, S. M. Hollen, L. Cao, Y. Cui, J. A. Gupta, H. R. Gutiérrez, T. F. Heinz, S. S. Hong, J. Huang, A. F. Ismach, E. Johnston-Halperin, M. Kuno, V. V. Plashnitsa, R. D. Robinson, R. S. Ruoff, S. Salahuddin, J. Shan, L. Shi, M. G. Spencer, M. Terrones, W. Windl and J. E. Goldberger, *ACS Nano*, 2013, **7**, 2898-2926.
2. G. Fiori, F. Bonaccorso, G. Iannaccone, T. Palacios, D. Neumaier, A. Seabaugh, S. K. Banerjee and L. Colombo, *Nat. Nanotechnol.*, 2014, **9**, 768-779.
3. F. H. L. Koppens, T. Mueller, P. Avouris, A. C. Ferrari, M. S. Vitiello and M. Polini, *Nat. Nanotechnol.*, 2014, **9**, 780-793.
4. O. Lopez-Sanchez, D. Lembke, M. Kayci, A. Radenovic and A. Kis, *Nat. Nanotechnol.*, 2013, **8**, 497-501.
5. K. Kang, S. Xie, L. Huang, Y. Han, P. Y. Huang, K. F. Mak, C.-J. Kim, D. Muller and J. Park, *Nature*, 2015, **520**, 656-660.
6. X. Cui, G.-H. Lee, Y. D. Kim, G. Arefe, P. Y. Huang, C.-H. Lee, D. A. Chenet, X. Zhang, L. Wang, F. Ye, F. Pizzocchero, B. S. Jessen, K. Watanabe, T. Taniguchi, D. A. Muller, T. Low, P. Kim and J. Hone, *Nat. Nanotechnol.*, 2015, **10**, 534-540.
7. J. S. Ross, P. Klement, A. M. Jones, N. J. Ghimire, J. Yan, D. G. Mandrus, T. Taniguchi, K. Watanabe, K. Kitamura, W. Yao, D. H. Cobden and X. Xu, *Nat. Nanotechnol.*, 2014, **9**, 268-272.
8. G. Su, V. G. Hadjiev, P. E. Loya, J. Zhang, S. Lei, S. Maharjan, P. Dong, P. M. Ajayan, J. Lou and H. Peng, *Nano Lett.*, 2015, **15**, 506-513.
9. Z. Wang, K. Xu, Y. Li, X. Zhan, M. Safdar, Q. Wang, F. Wang and J. He, *ACS Nano*, 2014, **8**, 4859-4865.
10. A. Allain and A. Kis, *ACS Nano*, 2014, **8**, 7180-7185.
11. Y.-F. Lin, Y. Xu, S.-T. Wang, S.-L. Li, M. Yamamoto, A. Aparecido-Ferreira, W. Li, H. Sun, S. Nakaharai, W.-B. Jian, K. Ueno and K. Tsukagoshi, *Adv. Mater.*, 2014, **26**, 3263-3269.
12. T. S. Pan, D. De, J. Manongdo, A. M. Guloy, V. G. Hadjiev, Y. Lin and H. B. Peng, *Appl. Phys. Lett.*, 2013, **103**, 093108.

View Article Online
DOI: 10.1039/C5NR05989E

13. K.-M. Chung, D. Wamwangi, M. Woda, M. Wuttig and W. Bensch, *J. Appl. Phys.*, 2008, **103**, 083523.
14. C. Ling, Y. Huang, H. Liu, S. Wang, Z. Fang and L. Ning, *J. Phys. Chem. C*, 2014, **118**, 28291-28298.
15. Y. Su, M. A. Ebrish, E. J. Olson and S. J. Koester, *Appl. Phys. Lett.*, 2013, **103**, 263104.
16. Z. Fang, S. Hao, L. Long, H. Fang, T. Qiang and Y. Song, *CrystEngComm*, 2014, **16**, 2404-2410.
17. P. A. Fernandes, M. G. Sousa, P. M. P. Salome, J. P. Leitao and A. F. da Cunha, *CrystEngComm*, 2013, **15**, 10278-10286.
18. P. Ramasamy, P. Manivasakan and J. Kim, *CrystEngComm*, 2015, **17**, 807-813.
19. C. H. de Groot, C. Gurnani, A. L. Hector, R. Huang, M. Jura, W. Levason and G. Reid, *Chem. Mat.*, 2012, **24**, 4442-4449.
20. L. Huang, Y. Yu, C. Li and L. Cao, *J. Phys. Chem. C*, 2013, **117**, 6469-6475.
21. S. Zhao, H. Wang, Y. Zhou, L. Liao, Y. Jiang, X. Yang, G. Chen, M. Lin, Y. Wang, H. Peng and Z. Liu, *Nano Res.*, 2015, **8**, 288-295.
22. H. R. Chandrasekhar, R. G. Humphreys, U. Zwick and M. Cardona, *Phys. Rev. B*, 1977, **15**, 2177-2183.
23. C. Julien, M. Eddrief, I. Samaras and M. Balkanski, *Mater. Sci. Eng., B*, 1992, **15**, 70-72.
24. C. Li, L. Huang, G. P. Snigdha, Y. Yu and L. Cao, *ACS Nano*, 2012, **6**, 8868-8877.
25. R. C. Sharma and Y. A. Chang, *Bulletin of Alloy Phase Diagrams*, 1986, **7**, 68-72.
26. J. V. Lauritsen, J. Kibsgaard, S. Helveg, H. Topsøe, B. S. Clausen, E. Lægsgaard and F. Besenbacher, *Nat. Nanotechnol.*, 2007, **2**, 53-58.
27. A. M. van der Zande, P. Y. Huang, D. A. Chenet, T. C. Berkelbach, Y. You, G.-H. Lee, T. F. Heinz, D. R. Reichman, D. A. Muller and J. C. Hone, *Nat. Mater.*, 2013, **12**, 554-561.
28. Q. Feng, N. Mao, J. Wu, H. Xu, C. Wang, J. Zhang and L. Xie, *ACS Nano, 2015, **9**, 7450-7455*.
29. S. Wang, Y. Rong, Y. Fan, M. Pacios, H. Bhaskaran, K. He and J. H. Warner, Chem. Mater., 2014, **26**, 6371-6379.
30. X. Xie, S.-Y. Kwok, Z. Lu, Y. Liu, Y. Cao, L. Luo, J. A. Zapien, I. Bello, C.-S. Lee and S.-T. Lee, *Nanoscale*, 2012, **4**, 2914-2919.
31. M. Buscema, D. J. Groenendijk, S. I. Blanter, G. A. Steele, H. S. van der Zant and A. Castellanos-Gomez, *Nano Lett.*, 2014, **14**, 3347-3352.
32. W. Choi, M. Y. Cho, A. Konar, J. H. Lee, G. B. Cha, S. C. Hong, S. Kim, J. Kim, D. Jena and J. Joo, *Adv. Mater.*, 2012, **24**, 5832-5836.
33. J. Xia, X. Huang, L.-Z. Liu, M. Wang, L. Wang, B. Huang, D.-D. Zhu, J.-J. Li, C.-Z. Gu and X.-M. Meng, *Nanoscale*, 2014, **6**, 8949-8955.
34. W. Zhang, J. K. Huang, C. H. Chen, Y. H. Chang, Y. J. Cheng and L. J. Li, *Adv. Mater.*, 2013, **25**, 3456-3461.
35. N. Huo, S. Yang, Z. Wei, S.-S. Li, J.-B. Xia and J. Li, *Scientific reports, 2014, 4, 5209*.
36. E. Zhang, Y. Jin, X. Yuan, W. Wang, C. Zhang, L. Tang, S. Liu, P. Zhou, W. Hu and F. Xiu, *Adv. Funct. Mater., 2015, 25, 4076-4082*.